Computer Assisted Mechanics and Engineering Sciences, 6: 361–368, 1999.

Comparison of numerical and experimental results of structronic plate and shell structures

Heinz Köppe, Ulrich Gabbert, Friedmann Laugwitz and Christian-Toralf Weber
Institut für Mechanik, Otto-von-Guericke-Universität Magdeburg
D-39106 Magdeburg, Universitätsplatz 2

(Received March 8, 1999)

In the paper a general purpose finite element software for the simulation of piezoelectric materials and structronic (structure and electronic) systems is presented. The equations of coupled electromechanical problems are given in a weak form, which are the basis of the development of 1D, 2D, 3D as well as multilayered composite shell elements. The smart structures finite element code includes static and dynamic analysis, where also controlled problems can be simulated. Two test examples are presented to compare the numerical results with measurements.

1. Introduction

In many branches of engineering lightweight design has become very important to reduce the mass and the energy consumption and to increase simultaneously the safety, integrity and environmental compatibility of a system. To meet these opposite objectives adaptive structural concepts have attracted increasing attention. These concepts are characterized by a synergistic integration of active (smart) materials, structures, sensors, actuators, and control electronic to an adaptive system. The potential uses of such concepts cover the entire range from mechanical engineering, aerospace engineering and civil engineering to manufacturing, transportation, robotics, medicine etc.

The use of plate and shell structures as basic components of such adaptive systems is very common. Such smart material systems often consist of different layers of passive and active materials, e.g. steel or aluminium sheets attached with piezoceramics, fiber reinforced composites with embedded piezoelectric wafers etc. [5, 6, 9, 11].

The global behavior of piezoelectric smart structures can be modeled with sufficient accuracy by the linearized coupled electromechanical constitutive equations. However, it is generally recognized that analytical solutions of the coupled electro-mechanical field equations are limited to relatively simple geometry and boundary conditions. In practical applications, finite element (FE) techniques provide the versatility in modeling, simulation, analysis and optimal design of real engineering adaptive structures. The paper gives an overview about our finite element simulation tool. Then two examples are presented from a number of test examples which we have investigated recently by numerical as well as experimental methods.

2. Governing equations of the electromechanical problem

The following derivation of the electromechanical fundamental relations is based on conventional formulations and notations of the theory of elasticity. In the sense of the principle of virtual work extended by the electrical part we can multiply these equations with a virtual displacement $\delta\mathbf{u}$ and with a virtual electric potential $\delta\Phi$, respectively. Integration over the entire domain and the surface

with applied loads, respectively, provides the coupled electromechanical functional

$$\chi = \int_V \delta\mathbf{u}^T \left(\mathbf{B}_u^T\boldsymbol{\sigma} + \bar{\mathbf{u}} - \rho\ddot{\mathbf{u}}\right) \mathrm{d}V + \int_V \delta\boldsymbol{\Phi} \left(\mathbf{B}_\Phi^T\mathbf{D}\right) \mathrm{d}V - \int_{O_q} \delta\mathbf{u}_q^T \left(\bar{\mathbf{t}}-\mathbf{t}\right) \mathrm{d}O - \int_{O_Q} \delta\boldsymbol{\Phi} \left(\bar{Q}-Q\right) \mathrm{d}O = 0 \tag{1}$$

with the stress vector σ, the body force vector $\bar{\mathbf{p}}$, the electrical displacement vector $\mathbf{D}$, the vector of applied surface traction $\bar{\mathbf{t}}$, the vector of applied surface charge $\bar{Q}$ and the density ρ. The linear coupled electromechanical constitutive equations have the form

$$\boldsymbol{\sigma} = \mathbf{C}\boldsymbol{\varepsilon} - \mathbf{e}E, \qquad \mathbf{D} = \mathbf{e}^T\boldsymbol{\varepsilon} + \boldsymbol{\kappa}\mathbf{E} \tag{2}$$

with the (6x6) elasticity matrix $\mathbf{C}$, the (6x3) piezoelectric matrix $\mathbf{e}$, the (3x3) dielectric matrix $\boldsymbol{\kappa}$, the strain vector $\boldsymbol{\sigma}$ and the electric field vector $\mathbf{E}$. In a preliminary polarised piezoelectric ceramic, where the direction of the polarisation at each point of the body is assumed to be direction 3 of a local Cartesian co-ordinate system, the material tensors are reduced to c_{11}, c_{12}, c_{13}, c_{33}, c_{44}, c_{66}, e_{31}, e_{33}, e_{15}, κ_{11}, κ_{33}, where the five independent elastic constants are measured under constant (or vanishing) electric field, and the three piezoelectric constants and the two dielectric constants are measured under constant (or vanishing) deformation.

Introducing equations (2) into equation (1) and using partial integration, the Gaussian integral theorem, the strain-displacement relationship $\boldsymbol{\varepsilon} = \mathbf{B}_u\mathbf{u}$ and the analogous relationship for the electric field $\mathbf{E} = -\mathbf{B}_\Phi\boldsymbol{\Phi}$, we get a suitable form of the functional (1) to derive finite element matrices as

$$\begin{aligned}\chi = &\int_V \delta\mathbf{u}^T\rho\ddot{\mathbf{u}}\,\mathrm{d}V + \int_V (\mathbf{B}_u\delta\mathbf{u})^T\,\mathbf{C}B_u\mathbf{u}\,\mathrm{d}V + \int_V (\mathbf{B}_u\delta\mathbf{u})^T\,\mathbf{e}B_\Phi\boldsymbol{\Phi}\,\mathrm{d}V \\ &+ \int_V (\mathbf{B}_\Phi\delta\boldsymbol{\Phi})^T\,\mathbf{e}^T\mathbf{B}_u\mathbf{u}\,\mathrm{d}V - \int_V (\mathbf{B}_\Phi\delta\boldsymbol{\Phi})^T\,\boldsymbol{\kappa}\mathbf{B}_\Phi\boldsymbol{\Phi}\,\mathrm{d}V \\ &- \int_V \delta\mathbf{u}^T\bar{\mathbf{p}}\,\mathrm{d}V - \int_{O_q} \delta\mathbf{u}^T\bar{\mathbf{t}}\,\mathrm{d}O - \int_{O_Q} \delta\boldsymbol{\Phi}\bar{Q}\,\mathrm{d}O = 0\end{aligned} \tag{3}$$

3. Finite element formulation and piezoelectric element library

For finite element discretization we approximate the mechanical displacements and the electric potential in a finite element by using the interpolation functions G_L

$$\mathbf{u}_i = \sum_{L=1}^{N} G_L\mathbf{u}_{il}, \qquad \boldsymbol{\Phi} = \sum_{L=1}^{N} G_L\boldsymbol{\Phi}_L, \tag{4}$$

where N is the number of element nodes and L is the nodal index. For an electromechanical finite element we extend the mechanical element nodal vector $\mathbf{q}_e$ by adding the electric potential Φ to each node

$$\mathbf{q}_e^T = \left[\ \mathbf{u}_1^T \,\middle|\, \boldsymbol{\Phi}_1 \,\middle|\, \cdots \,\middle|\, \mathbf{u}_L^T \,\middle|\, \boldsymbol{\Phi}_L \,\middle|\, \cdots \,\middle|\, \mathbf{u}_N^T \,\middle|\, \boldsymbol{\Phi}_N\ \right]. \tag{5}$$

To express $\mathbf{e}$ and $\mathbf{E}$ we need the derivatives of the shape functions G

$$\begin{bmatrix} \boldsymbol{\varepsilon} \\ \mathbf{E} \end{bmatrix} = \left[\begin{array}{cc|cc|c|cc} \mathbf{B}_{uG_1} & \mathbf{0} & \mathbf{B}_{uG_2} & \mathbf{0} & \cdots & \mathbf{B}_{uG_N} & \mathbf{0} \\ \mathbf{0} & \mathbf{B}_{\Phi G_1} & \mathbf{0} & \mathbf{B}_{\Phi G_2} & \cdots & \mathbf{0} & \mathbf{B}_{\Phi G_N} \end{array}\right] \tag{6}$$

where

$$\mathbf{B}_{uG_L} = \mathbf{B}_uG_L\,, \qquad \mathbf{B}_{\Phi G_L} = \mathbf{B}_\Phi G_L\,. \tag{7}$$

Introducing these approximations into equation (3) and using the fundamental lemma of the calculus of variation provide the relations for one finite element (index e) in the form of a differential equation system

$$\mathbf{M}_e\ddot{\mathbf{q}}_e + \mathbf{R}_e\dot{\mathbf{q}}_e + \mathbf{K}_e\mathbf{q}_e = \mathbf{f}_e\,, \tag{8}$$

where $\mathbf{M}_e$ is the element mass matrix, $\mathbf{K}_e$ is the element stiffness/electric matrix and $\mathbf{f}_e$ is the element load vector, respectively.

$$\begin{aligned}
\mathbf{M}_e &= \int_{V_e} \rho\mathbf{G}^T\mathbf{G}\,\mathrm{d}V,\\
\mathbf{K}_e &= \int_{V_e} \mathbf{B}_{u\Phi G}^T \begin{bmatrix} \mathbf{C} & \mathbf{e} \\ \mathbf{e}^T & \boldsymbol{\kappa} \end{bmatrix} \mathbf{B}_{u\Phi G}\,\mathrm{d}V,\\
\mathbf{f}_e &= \begin{bmatrix} \int\limits_{V_e} \mathbf{G}^T\bar{\mathbf{p}}\,\mathrm{d}V + \int\limits_{O_{eq}} \mathbf{G}^T\bar{\mathbf{t}}\,\mathrm{d}O \\ \int\limits_{O_{eQ}} \mathbf{G}^T\bar{Q}\,\mathrm{d}O \end{bmatrix}
\end{aligned} \tag{9}$$

In addition, a rate-dependent damping matrix $\mathbf{R}_e$ can be included to take into account damping effects as well. Based on the theoretical background given above a library of piezoelectric finite

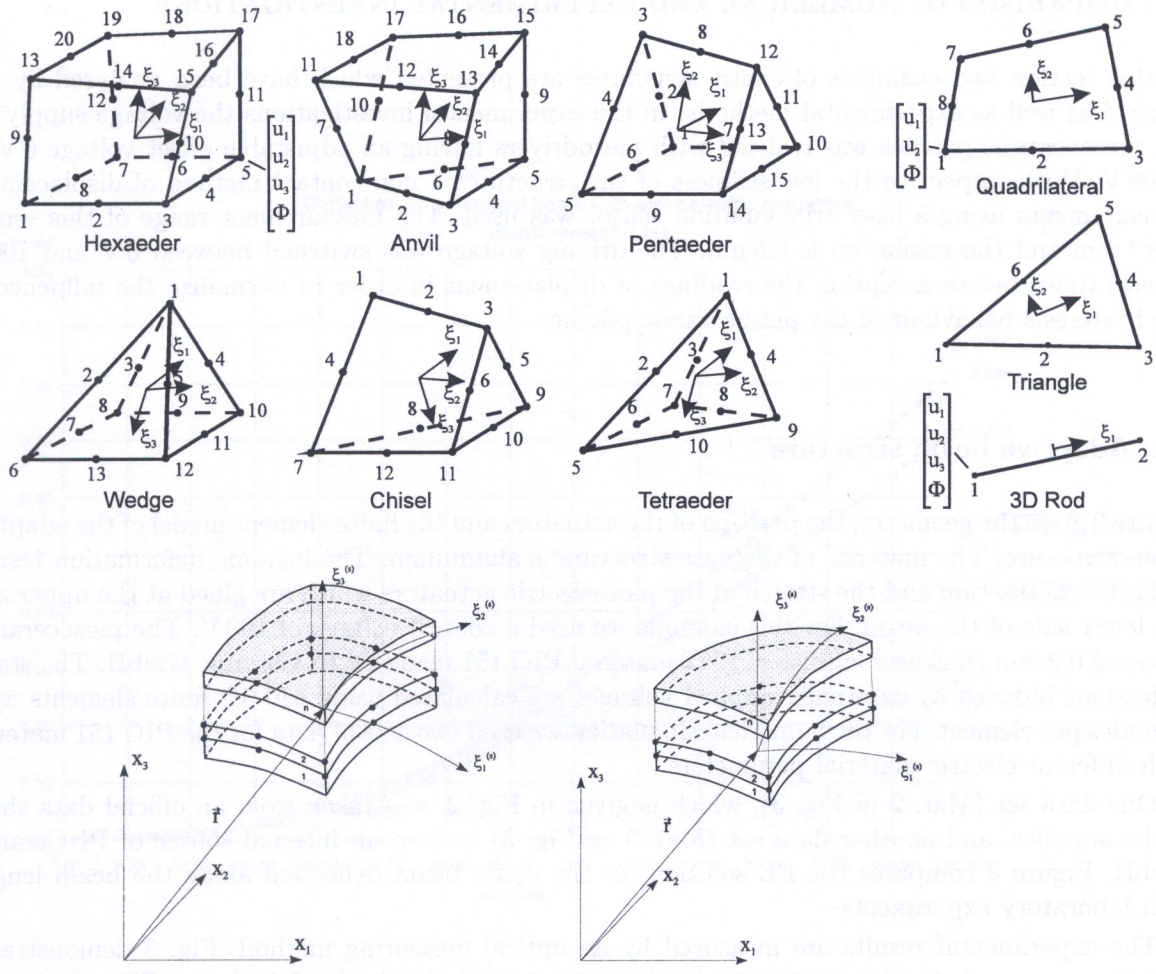

Fig. 1. Piezoelectric finite element library

elements has been developed (Fig. 1) and testwise implemented in the general purpose finite element code COSAR. The shape functions of the elements can be linear or quadratic, and the isoparametric element concept has been used to approximate the element geometry. The solid element family consists of a basic brick element (hexahedron) and some special degenerate elements which have been derived by collapsing nodes [1]. The quadrilateral and triangular multilayered shell elements shown in Fig. 1 have been developed on the basis of a triangular piezoelectric shell element by H.S. Tzou & R. Ye [12]. We added a quadrilateral element and extended the geometry approximation by an isoparametric description, and consequently, complex laminated structures can be modelled by these elements [8].

Thin shell assumptions can be included for the shell as a whole or several layers, and consequently, the number of degrees of freedom can be reduced by constraint conditions. Global and local effects such as the transfer behavior of active to passive parts of a structure or delamination propagation can also be investigated effectively by these elements [3]. Piezoelectric elements and conventional mechanical elements can be combined in one model.

This technique provides an efficient way to analyse complex adaptive structures which contain in general only a few special piezoelectric actuators or sensors located at special parts. The finite element code has the capability to use a substructure technique, and consequently, it is possible to separate mechanical and piezoelectric structures, and only the hyperstructure has merged DOF's.

4. Comparison of numerical and experimental investigations

In this section two examples of smart structures are presented which have been analysed by numerical as well as experimental methods. In the experimental investigations the voltage supply for the piezoceramic patches was realized with piezodrivers having an adjustable offset voltage 0 V to +100 V. With respect to the low stiffness of the structures a non contact method of displacement measurements using a laser triangulation sensor was used. The measurement range of this sensor is ±1 mm and the resolution is 0.5 μm. The driving voltage was switched between 0 V and 100 V several times before accepting the readings of displacement in order to normalize the influence of the hysteresis behaviour of the piezoceramic patches.

4.1. Adaptive beam structure

Figure 2 gives the geometry, the position of the actuators and the finite element model of the adaptive beam structure. The material of the base structure is aluminium. The bending deformation results from the contraction and the stretch of the piezoelectric actuators which are glued at the upper and the lower side of the beam. For this example we used a control voltage of 100 V. The piezoceramic layers of 0.2 mm thickness consist of PZT material PIC 151 made by PI Ceramic GmbH. The static deflections induced by externally applied voltages are calculated using 640 3D finite elements with 20 nodes per element. For the numerical simulation we used two sets of data for the PIC 151 material with different electric material parameters.

One data set (Mat. 2 in Fig. 3), which is given in Fig. 2, was taken from an official data sheet of the supplier, and another data set (Mat. 1 in Fig. 3) is from an internal source of PI Ceramic GmbH. Figure 3 compares the FE solution for the static beam deflection along the beam length with laboratory experiments.

The experimental results are measured by an optical measuring method. Fig. 3 demonstrates that the measured displacements are greater than the results obtained from the FE calculation. Finally, the two different sets of material parameters result in a maximum error of the tip deflection with respect to the experimental results of 16.8% (Mat. 2) and 4.9% (Mat. 1).

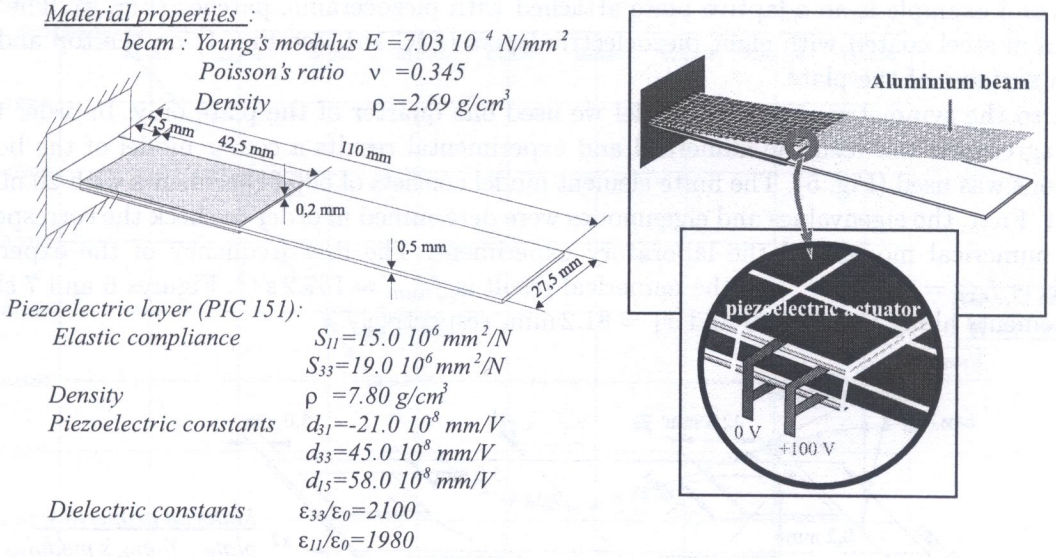

Fig. 2. Model of a clamed beam with piezoelectric actuators

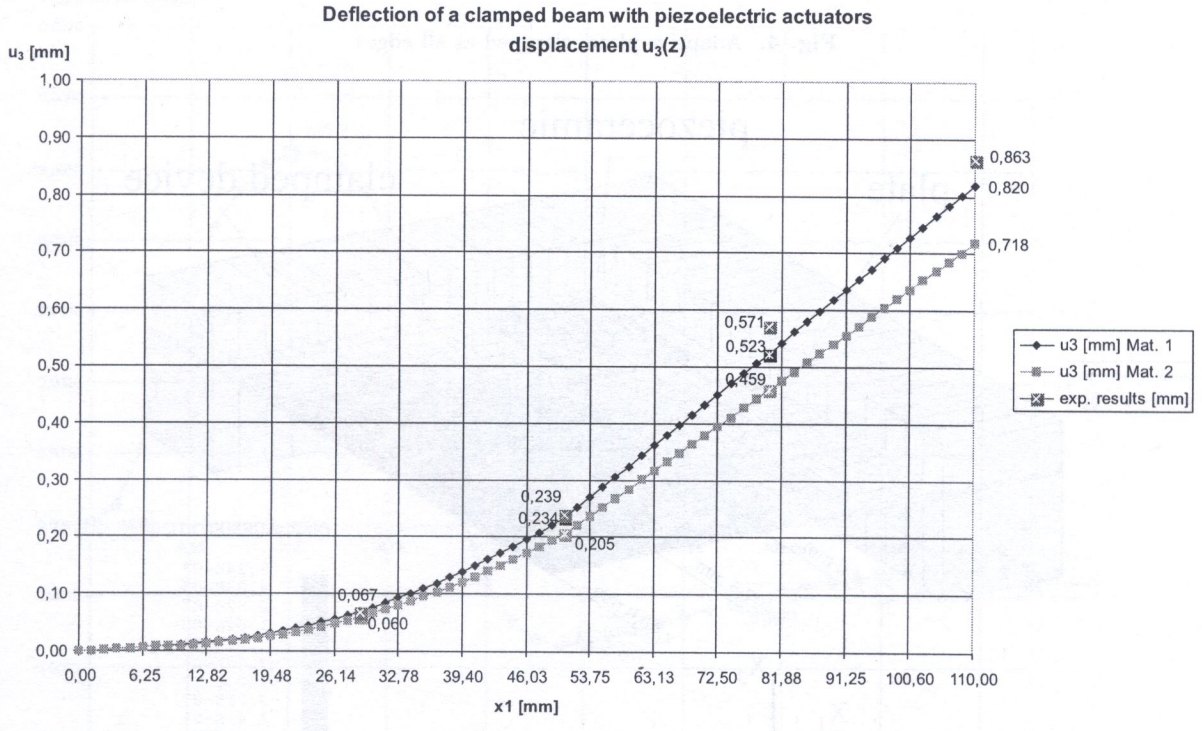

Fig. 3. Comparison between numerical and experimental results

4.2. Clamped adaptive plate

The second example is an adaptive plate attached with piezoceramic patches (Fig. 4). The plate is made from steel coated with eight piezoelectric layers (PIC 151, see Fig. 1) on the top and on the bottom surfaces of the plate.

Due to the symmetry of the FE model we used one quarter of the plate only. In order to get a better agreement between the numerical and experimental results a coarse model of the boundary conditions was used (Fig. 5). The finite element model consists of 506 3D elements with 20 nodes per element. First, the eigenvalues and eigenmodes were determined in order to check the correspondence of the numerical model and the laboratory experiment. The first frequency of the experimental analysis is $f_{exp} = 163.5\,\mathrm{s}^{-1}$, and the numerical result is $f_{num} = 167.2\,\mathrm{s}^{-1}$. Figures 6 and 7 show the displacements along line $x_1 = 0$ and $x_1 = 81.2\,\mathrm{mm}$, respectively.

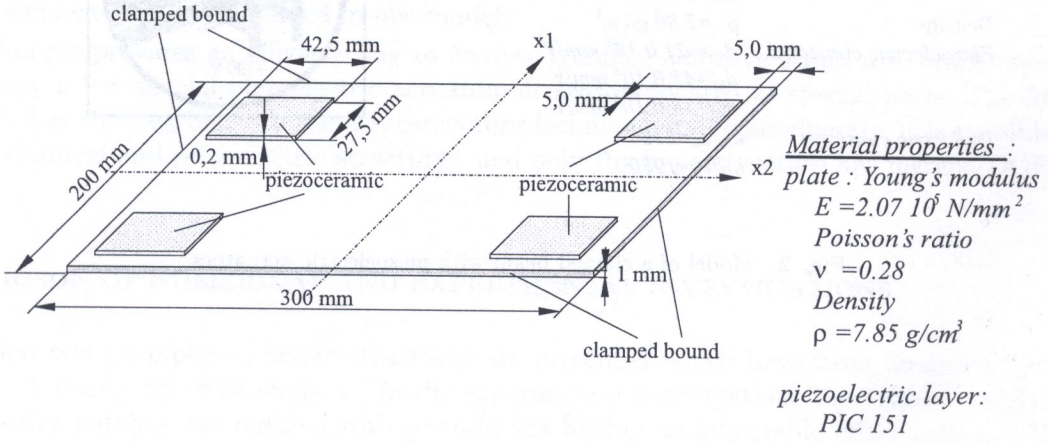

Fig. 4. Adaptive plate, clamped at all edges

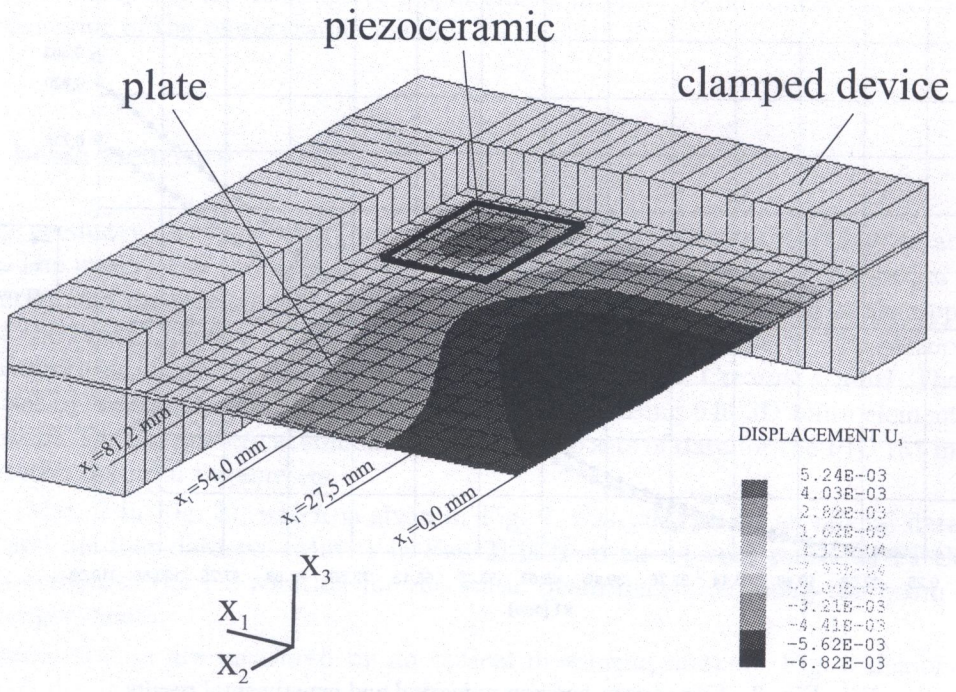

Fig. 5. FE model and displacement results for the clamped plate

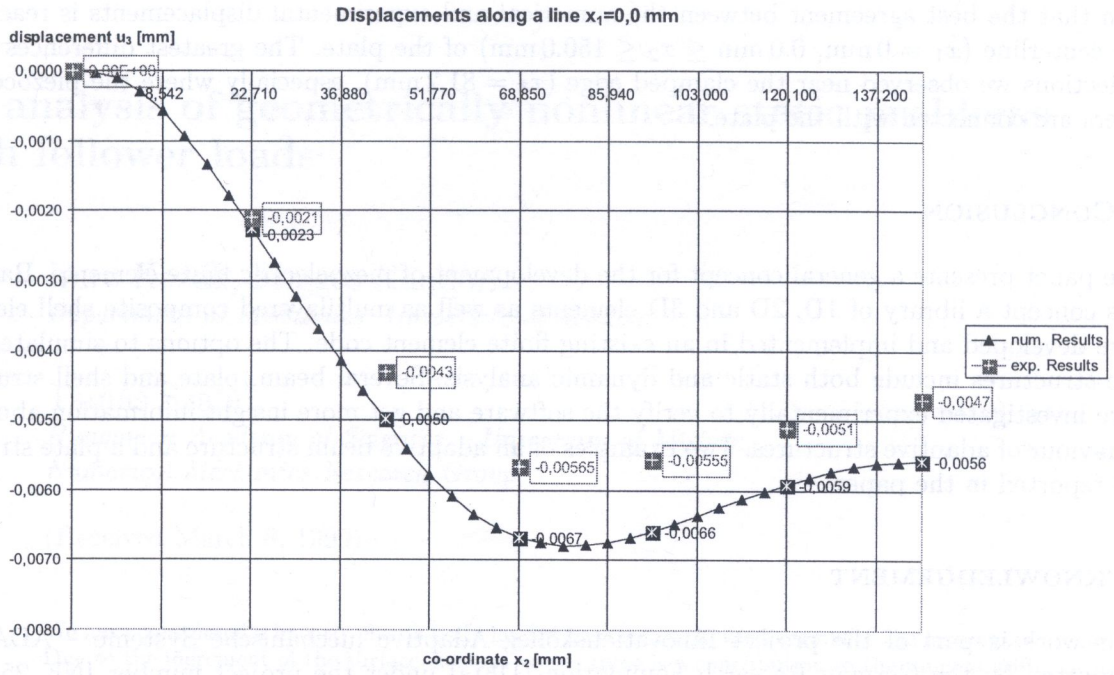

Fig. 6. Comparison of numerical and experimental results at $x_1 = 0\,\mathrm{mm}$

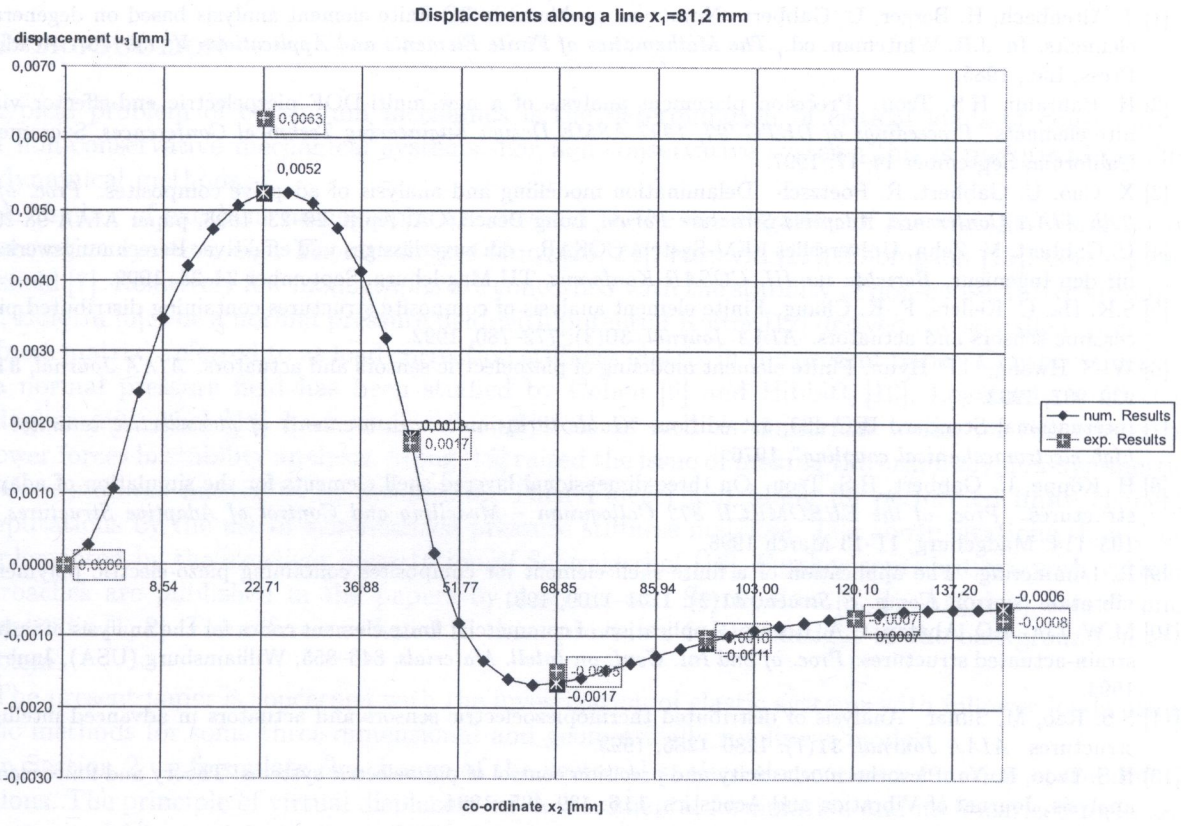

Fig. 7. Comparison of numerical and experimental results at $x_1 = 81.2\,\mathrm{mm}$

The experimental data in Figs. 6 and 7 are mean values obtained from several tests. It can be seen that the best agreement between the numerical and experimental displacements is reached in the centerline ($x_1 = 0\,\text{mm}$, $0.0\,\text{mm} \leq x_2 \leq 150.0\,\text{mm}$) of the plate. The greatest differences in the deflections we observed near the clamped edge ($x_1 = 81.2\,\text{mm}$), especially where the piezoceramic layers are connected with the plate.

5. Conclusion

The paper presents a general concept for the development of piezoelectric finite elements. Based on this concept a library of 1D, 2D and 3D elements as well as multilayered composite shell elements were developed and implemented in an existing finite element code. The options to simulate adaptive structures include both static and dynamic analysis. Several beam, plate and shell structures were investigated experimentally to verify the software and get more insight information about the behaviour of adaptive structures. Two examples of an adaptive beam structure and a plate structure are reported in the paper.

Acknowledgement

This work is part of the project Innovationskolleg Adaptive mechanische Systeme – ADAMES, supported by the German Research Foundation (DFG) under the project number INK 25/A1-1. This support is gratefully acknowledged.

References

[1] J. Altenbach, H. Berger, U. Gabbert. Numerical problems in 3D finite element analysis based on degenerated elements. In: J.R. Whiteman. ed., *The Mathematics of Finite Elements and Applications V*, 459–467. Academic Press, Inc., 1985.

[2] H. Bahrami, H.S. Tzou. Precision placement analysis of a new multi-DOF piezoelectric end-effector via finite elements. *Proceedings of DETC '97, 1997 ASME Design Engineering Technical Conferences*, Sacramento, California, September 14–17, 1997.

[3] X. Cao, U. Gabbert, R. Poetzsch. Delamination modelling and analysis of adaptive composites. *Proc. of the 39th AIAA Conference, Adaptive Structure Forum*, Long Beach, CA, April, 20–23, 1998, paper AIAA-98-2046.

[4] U. Gabbert, M. Zehn. Universelles FEM-System COSAR – ein zuverlässiges und effektives Berechnungswerkzeug für den Ingenieur. *Berichte zur III. COSAR-Konferenz*, TU Magdeburg, September 24–25, 1992.

[5] S.K. Ha, C. Keilers, F.-K. Chang. Finite element analysis of composite structures containing distributed piezoceramic sensors and actuators. *AIAA Journal*, **30**(3): 772–780, 1992.

[6] W.-S. Hwang, C.P. Hyun. Finite element modeling of piezoelectric sensors and actuators. *AIAA Journal*, **31**(5): 930–937, 1993.

[7] International Standard IEC 483, 1st edition, *"Guide to dynamic measurements of piezoelectric ceramics with high electromechanical coupling"*, 1976.

[8] H. Köppe, U. Gabbert, H.S. Tzou. On three-dimensional layered shell elements for the simulation of adaptive structures. *Proc. of the EUROMECH 373 Colloquium – Modelling and Control of Adaptive Structures*, pp. 103–114, Madgeburg, 11–13 March 1998.

[9] R. Lammering. The application of a finite shell element for composites containing piezo-electric polymers in vibration control. *Comp. & Struct.*, **41**(5): 1101–1109, 1991.

[10] M.W. Lin, A.O. Abatan, C.A. Rogers. Application of commercial finite element codes for the analysis of induced strain-actuated structures. *Proc. of 2nd Int. Conf. on Intell. Materials*, 846–855, Williamsburg (USA), June 5–8, 1994.

[11] S.S. Rao, M. Sunar. Analysis of distributed thermopiezoelectric sensors and actuators in advanced intelligent structures. *AIAA Journal*, **31**(7): 1280–1286, 1993.

[12] H.S. Tzou, R. Ye. Piezothermoelasticity and precision control of piezoelectric systems: Theory and finite element analysis. Journal of Vibration and Acoustics, **116**: 489–495, 1994.